HHS Public Access

Author manuscript

Nat Immunol. Author manuscript; available in PMC 2015 July 01.

Published in final edited form as:

Nat Immunol. 2015 January ; 16(1): 67–74. doi:10.1038/ni.3046.

The methyltransferase Setdb2 mediates virus-induced susceptibility to bacterial superinfection

Christopher Schliehe[1], **Elizabeth K. Flynn**[#2,+], **Bojan Vilagos**[#1], **Udochuku Richson**[#1], **Savitha Swaminanthan**[3], **Berislav Bosnjak**[4], **Lisa Bauer**[1], **Richard K. Kandasamy**[1], **Isabel M. Griesshammer**[1,++], **Lindsay Kosack**[1], **Frank Schmitz**[3], **Vladimir Litvak**[5], **James Sissons**[3], **Alexander Lercher**[1], **Anannya Bhattacharya**[1], **Kseniya Khamina**[1], **Anna L. Trivett**[2], **Lino Tessarollo**[2], **Ildiko Mesteri**[6], **Anastasiya Hladik**[1,7], **Doron Merkler**[8,9], **Stefan Kubicek**[1], **Sylvia Knapp**[1,7], **Michelle M. Epstein**[4], **David E. Symer**[#2,10], **Alan Aderem**[#3], and **Andreas Bergthaler**[1,§]

[1] CeMM Research Center for Molecular Medicine of the Austrian Academy of Sciences, Vienna, Austria [2] Center for Cancer Research, National Cancer Institute, Frederick, MD, USA [3] Seattle Biomedical Research Institute, Seattle, WA, USA [4] Department of Dermatology, DIAID, Experimental Allergy, Medical University of Vienna, Vienna, Austria [5] University of Massachusetts, Worcester, MA, USA [6] Department of Pathology, Medical University of Vienna, Vienna, Austria [7] Department of Medicine 1, Medical University of Vienna, Vienna, Austria [8] Department of Pathology and Immunology, Division of Clinical Pathology, University & University Hospital of Geneva, Geneva, Switzerland [9] Department of Neuropathology, Georg-August-University Goettingen, Germany [10] Ohio State University Comprehensive Cancer Center, Columbus, OH, USA

[#] These authors contributed equally to this work.

Abstract

Immune responses are tightly regulated to ensure efficient pathogen clearance while avoiding tissue damage. Here we report that SET domain bifurcated 2 (Setdb2) was the only protein lysine

[§] Corresponding author: abergthaler@cemm.oeaw.ac.at.
[+]Present address: GeneDx Inc., Gaithersburg, MD, USA.
[++]Present address: Institute of Molecular Biotechnology (IMBA) of the Austrian Academy of Sciences, Vienna, Austria.

COMPETING FINANCIAL INTERESTS
Patent pending (C. S. and A.B.).

Microarray accession numbers
The raw data from the array and RNAseq data are deposited at ArrayExpress (http://www.ebi.ac.uk/arrayexpress/) with accession numbers E-MTAB-2845 and EMTAB-2263.

Authors contributions:
C.S. designed experiments, performed *in vitro* and *in vivo* studies and wrote the manuscript; E.K.F., A.L.T., L.T. and D.E.S. generated the Setdb2$^{GT/GT}$ mouse and provided advice; U.R. performed *in vitro* experiments and generated the monoclonal antibody; B.V. performed ChIP, flow cytometry and *in vivo* experiments and created illustrations; S.S., L.B., I.M.G., L.K., A.L., A.Bh. and K.K. performed *in vitro* experiments. B.B. and M.M.E. performed *in vivo* experiments and provided advice. R.K.K. performed bioinformatics analyses. F.S., V.L., J.S. and S.Ku. provided reagents and/or advice. D.M., I.M., A.H. and S.Kn. did histological analyses and provided reagents and/or advice. D.E.S. and A.A. co-supervised the study and provided reagents and advice. A.B. supervised the study, designed experiments, performed *in vitro* and *in vivo* experiments and wrote the manuscript.

methyltransferase induced during influenza virus infection. Setdb2 expression depended on type-I interferon signaling and it repressed the expression of the neutrophil attractant *Cxcl1* and other NF-κB target genes. This coincided with Setdb2 occupancy at the *Cxcl1* promoter, which in the absence of Setdb2 displayed reduced H3K9 tri-methylation. *Setdb2* hypomorphic gene-trap mice exhibited increased neutrophil infiltration in sterile lung inflammation and were less sensitive to bacterial superinfection upon influenza virus infection. This suggests that a Setdb2-mediated regulatory crosstalk between the type-I interferon and NF-κB pathways represents an important mechanism for virus-induced susceptibility to bacterial superinfection.

Secondary bacterial pneumonia plays a predominant role in the morbidity of seasonal and pandemic influenza virus infection, thereby representing a significant clinical as well as socioeconomic challenge [1, 2, 3]. Virus-induced immune responses are thought to be involved in the pathogenesis of bacterial superinfections, yet the molecular mechanisms remain poorly understood [4]. Pathogen recognition by receptors such as toll-like receptors (TLRs) [5], lead to the induction of two major pathways; type-I interferon (IFN) and nuclear factor kappa B (NF-κB) signaling. The transcription of type I IFNs is regulated by the family of interferon regulatory factors (IRFs) [6]. Secreted IFNs bind to the ubiquitously expressed heteromeric receptor IFNα/β receptor 1 (IFNAR1) and IFNAR2, which results in the expression of a large number of interferon-stimulated genes (ISGs). Many ISGs encode effector proteins, which mediate the defense against viruses and other pathogens [7, 8]. The same triggering of TLRs can lead to the activation and nuclear translocation of NF-κB proteins, which in turn induce the expression of pro-inflammatory genes involved in antibacterial defense [5, 9]. Type-I IFN and NF-κB signaling are subjected to multiple layers of regulation, which are required to maintain a balance between effective pathogen clearance, the prevention of tissue damage and disease tolerance [10, 11, 12]. This is of particular relevance in superinfections, where virus-induced host responses can lead to an increased susceptibility to bacterial infections through type I IFN-mediated interference with NF-κB signaling [4, 13, 14, 15].

Immune responses are shaped by chromatin modifications [16, 17, 18, 19]. Here, we have identified and functionally characterized the protein lysine methyltransferase (PKMT) SET domain bifurcated 2 (Setdb2, Uniprot: Q8C267) as an IFN-stimulated protein that modulates the expression of a subset of NF-κB target genes. Setdb2 belongs to the *SUV39* gene family, whose members share a Suvar 3-9/Enhancer-ofzeste/Trithorax (SET) domain that transfers methyl residues from S-adenosylmethionine to the amino group of target lysines thereby catalyzing H3K9 methylation [20]. Setdb1, the closest related family member of Setdb2, is involved in pro-viral silencing, genomic stability and the onset of cancer [21, 22]. To date, functional roles for Setdb2 have been implicated in embryonic development and cell division [23, 24, 25]. In this study we report a role for Setdb2 as a critical IFN-stimulated regulator of the immune system, which contributes to the molecular mechanisms of virus-induced susceptibility to bacterial superinfection.

RESULTS

Influenza virus infection induces Setdb2 expression

To identify novel regulatory immune mechanisms that are involved in virus-induced susceptibility to bacterial superinfection, we infected wild type (WT) mice with influenza virus and collected lung tissue at 18 hours after infection. At this early time point, the distribution of viral antigen was limited to a small percentage of epithelial cells (**Fig. 1a**). We next performed a global expression profiling of lung tissue from infected and uninfected WT mice (**Fig. 1b, Supplementary Table 1**). We identified more than 200 virus-induced genes with many of them being known ISGs [8]. A gene ontology (GO) analysis highlighted the enrichment of genes involved in IFN-mediated immune responses (**Supplementary Table 1**), which included the GO terms interferon alpha and interferon beta signaling (Reactome:M973, $p=0e^{0}$) and interferon-mediated immunity (Panther:BP00156, $p=1.50e^{-40}$) as well as chemokine signaling pathway (KEGG:M4844, $p=4.85e^{-14}$), toll-like receptor signaling pathway (KEGG:M3261, $p=7.89e^{-14}$), macrophage-mediated immunity (Panther:BD00155, $p=5.00e^{-12}$) and cytokine/chemokine-mediated immunity (Panther:BP00255, $p=1.70e^{-8}$). This was confirmed by the enrichment of transcription factor binding targets for *Irf1* (p-value $0e^{0}$), *Irf8* ($0e^{0}$), *Irf7* ($1.11e^{-16}$) and *Irf2* ($2.43e^{-11}$) (**Methods**). Next, we analyzed the expression of the mouse orthologs of the previously annotated PKMTs [26]. This revealed Setdb2 as the only statistically significant PKMT that was induced upon influenza virus infection (**Fig. 1b**, **Supplementary Table 1**).

Type-I interferon signaling drives Setdb2 expression

We identified several putative IRF binding sites by motif scanning of the Setdb2 gene (**Supplementary Table 2**, **Methods**). To study whether the induction of *Setdb2* depended on IFN signaling, we infected wild-type (WT) as well as *Ifnar1*$^{-/-}$, *Irf7*$^{-/-}$ and *Stat1*$^{-/-}$ mice, each of them lacking key molecules required for IFN signaling, with influenza virus. We collected lung tissue at 18 hours after infection and detected increased expression of *Setdb2* in infected WT lungs (**Fig. 1c**). In contrast, the induction of *Setdb2* was strongly reduced in *Ifnar1*$^{-/-}$ lungs, indicating that type I IFN signaling is essential for *Setdb2* up-regulation *in vivo*. A reduction of *Setdb2* expression was also observed in *Irf7*$^{-/-}$ and *Stat1*$^{-/-}$ mice (**Fig. 1c**). Similarly, infection of primary mouse bone marrow-derived macrophages (BMDMs) with influenza virus resulted in an IFNAR1-dependent up-regulation of *Setdb2* transcription (**Fig. 1d**). To investigate protein expression, we raised a monoclonal antibody (mAb) against the c-terminal region of mouse Setdb2 (clone 7H7F11, **Methods**). Consistent with RNA expression, we detected increased Setdb2 protein after infection of BMDMs in an IFNAR1-dependent manner (**Fig. 1d**). Detection of the known IFN-stimulated protein Zbp1 (alias DAI) served as a control. Stimulation of BMDMs with IFNβ (type I IFN), IFN-γ (type II IFN) or IFN-λ (type III IFN) revealed that Setdb2 and Zbp1 are induced by type I IFN as well as by type II IFN but not type III IFN (**Fig. 1e**). The induction of Setdb2 by type II IFN was partially dependent on IFNAR1, indicating a secondary requirement for endogenous type I IFN [27].

Next, we elucidated the mRNA and protein expression profiles of Setdb2 after stimulation of BMDMs with the TLR2 agonist Pam(3)CSK(4) (PAM3), the synthetic viral RNA analog

and TLR3 agonist polyinosinic-polycytidylic acid (poly(I:C)) and the TLR4 agonist lipopolysaccharide (LPS) [5]. Treatment of WT BMDMs resulted in up-regulation of *Setdb2* at the RNA and protein level (**Fig. 1f**). Again, this induction was entirely dependent on type I IFN signaling, as *Setdb2* was not induced in *Ifnar1*$^{-/-}$ BMDMs. The induction of *Setdb2* and *Zbp1* upon PAM3 stimulation was TLR2-dependent (**Supplementary Fig. 1**). In addition to Setdb2, stimulation of WT BMDMs with poly(I:C) led to induction of other PKMTs such as *Setd1b* and *Prdm1* (alias: *Blimp1)*, a well-studied regulator of B- and T-cells, that were however not altered upon influenza virus infection *in vivo* (**Supplementary Fig. 2, Supplementary Table 3, Fig. 1b**). Elevated expression of *Setdb2* mRNA in WT BMDMs persisted for at least 24 hours (**Supplementary Fig. 2**). Together, these data indicate that IFN signaling is required for the induction of Setdb2 both in viral infection and upon TLR stimulation.

Setdb2 modulates expression of NF-κB target genes

We generated *Setdb2* genetrap mice (*Setdb2*$^{GT/GT}$) to investigate the biological function of Setdb2 (**Supplementary Fig. 3** and **Methods**). Immunoblot analysis of spleen, lung and BMDMs showed a strong reduction of the Setdb2 protein in the hypomorphic *Setdb2*$^{GT/GT}$ mice compared to WT controls (**Fig. 2a**). Next, we compared the transcriptomes of poly(I:C)-stimulated WT and *Setdb2*$^{GT/GT}$ BMDMs by RNAseq. This revealed a significant enrichment of known NF-κB target genes among the up-regulated transcripts in *Setdb2*$^{GT/GT}$ BMDMs (p-value = 1.35×10^{-8}, **Fig. 2b**, **Supplementary Tables 4-5** and **Methods**). These NF-κB target genes represented a subset of genes including *Cxcl1, Il12b, S100a8/9, Lcn2, Cxcl2, Chi3l1* and *Ltf*, each of which has been implicated in antibacterial defense. Other established NF-κB regulated genes such as *Il6*, however, were not affected (**Supplementary Table 4**). Upstream activation of the NF-κB cascade as measured by IκBα degradation showed no difference between stimulated WT and *Setdb2*$^{GT/GT}$ BMDMs (**Supplementary Fig. 4**), suggesting that Setdb2 acts downstream of IκBα-mediated NF-κB activation.

One of the genes found with particularly high levels of expression in poly(I:C) stimulated *Setdb2*$^{GT/GT}$ BMDMs was *Cxcl1*. This encodes a key chemoattractant for neutrophils, a type of leukocyte shown to be critically involved in bacterial clearance in superinfection [13, 14, 15]. Thus, we decided to focus on the effects of Setdb2-mediated regulation of *Cxcl1*. Indeed, stimulation with different TLR agonists resulted in the induction of significantly more *Cxcl1* transcripts in *Setdb2*$^{GT/GT}$ BMDMs as compared to WT controls (**Fig. 2c**). This finding was confirmed at the level of protein secreted by BMDM (**Fig. 2d**). To investigate the effects of type I IFN signaling on *Cxcl1* expression, we stimulated BMDMs with poly(I:C) in the presence of IFNAR1-blocking antibodies. This led to diminished levels of *Setdb2* mRNA, which correlated inversely with the expression of *Cxcl1* mRNA (**Supplementary Fig. 5**). These differences were seen not only in WT but also in *Setdb2*$^{GT/GT}$ BMDMs, which may be due to the residual levels of Setdb2 in the *Setdb2*$^{GT/GT}$ BMDMs and/or another IFN-I driven Setdb2-independent pathway. Finally, infection with influenza virus strain PR8 led to increased CXCL1 expression in *Setdb2*$^{GT/GT}$ compared to WT BMDMs (**Fig. 2e, f**). These data suggest that Setdb2 is a negative regulator of a subset of NF-κB target genes.

Setdb2 mediates H3K9 tri-methylation at the *Cxcl1* promoter

Methyltransferases of the SUV39 family preferentially methylate the histone substrate H3K9 [20, 28]. Setdb2 was shown to catalyze the addition of the repressive mark H3K9me3 [23, 24]. We, therefore, hypothesized that Setdb2 would inhibit *Cxcl1* expression by introducing repressive marks in the *Cxcl1* promoter region. To test if Setdb2 was able to bind to the *Cxcl1* promoter, we used the Setdb2-specific mAb clone 7H7F11 to perform chromatin immunoprecipitation (ChIP) experiments. BMDMs were treated with poly(I:C) for two hours and Setdb2-specific enrichment of genomic DNA was quantified by real-time PCR. We found a significant enrichment of the promoter region and exon 1 of *Cxcl1* in Setdb2 ChIP assays in comparison to the promoter sequences of the constitutively expressed control gene *Actb* (**Fig. 3a**). This indicates that Setdb2 binds to the *Cxcl1* promoter.

Next, we addressed whether Setdb2 binding correlated with altered chromatin modifications. To test this, we performed H3K9me3 ChIP experiments in the presence or absence of poly(I:C) stimulation in either WT or *Setdb2*$^{GT/GT}$ BMDMs. Under unstimulated conditions, *Setdb2*$^{GT/GT}$ cells displayed less H3K9 tri-methylation compared to WT controls (**Fig. 3b**). This repressive mark was significantly increased at the *Cxcl1* promoter upon poly(I:C) stimulation of WT cells, which is consistent with the rapid induction but only transient expression of this gene (**Supplementary Fig. 6**). This increase of H3K9me3 was absent in *Setdb2*$^{GT/GT}$ cells. The promoter of the actively transcribed gene *Actb* had a low degree of H3K9 tri-methylation in both WT and *Setdb2*$^{GT/GT}$ BMDMs. Finally, we analyzed the presence of the activation mark H3K9ac and, as expected, found enrichment at the promoter of *Actb* **(Fig. 3c)**. Together, these data suggested that Setdb2 mediated the repression of *Cxcl1* expression at the chromatin level.

Setdb2 deficiency results in exacerbated lung inflammation

Experiments with *Setdb2*$^{GT/GT}$ BMDMs revealed an increased expression of CXCL1, which as a chemoattractant for neutrophils is important for efficient pathogen clearance as well as implicated in immunopathologies [29]. To corroborate our *in vitro* findings, we challenged WT and *Setdb2*$^{GT/GT}$ mice using a model of LPS-induced pulmonary neutrophilia. Four hours after an intranasal application of LPS, bronchoalveolar lavage fluid (BAL) was obtained to determine potential changes in CXCL1 secretion and cell infiltration. In addition, total RNA was extracted from lung tissue to analyze differential gene expression. This demonstrated increased levels of *Cxcl1* mRNA expression (**Fig. 4a**) and protein secretion (**Fig. 4b**) in *Setdb2*$^{GT/GT}$ mice. The CXCL1 increase was accompanied by elevated total cell infiltration (**Fig. 4c**) and neutrophilia in the airways as measured by cytospin **(Fig. 4d)**. Macrophage numbers were similar in WT and *Setdb2*$^{GT/GT}$ mice (**Fig. 4e**). We conclude that *Setdb2*$^{GT/GT}$ mice show increased lung infiltration of neutrophils in the early phase of inflammation.

Setdb2 mediates susceptibility to bacterial superinfection

The rapid recruitment of neutrophils by the early cytokine CXCL1 is crucial for the prevention of excessive lung inflammation as well as for the clearance of *Streptococcus pneumonia* (SP), the most common bacterial agent found in influenza virus-induced

superinfection [1, 14, 15, 30]. Therefore, we sought to investigate the response of *Setdb2*$^{GT/GT}$ mice in a superinfection model of SP after primary influenza virus infection.

Upon intranasal infection with influenza virus, *Setdb2*$^{GT/GT}$ mice induced more CXCL1 compared to WT controls (**Fig. 5a, b**). In the lung, CXCL1 is secreted by multiple cell types including alveolar macrophages [31]. Indeed, influenza virus infection of alveolar macrophages taken *ex vivo* from BAL fluid of *Setdb2*$^{GT/GT}$ mice expressed more CXCL1 compared to WT controls (**Supplementary Fig. 7**), implicating this cell population as one source of CXCL1 in our infection model *in vivo*. The protein expression of other inflammatory mediators such as Cxcl2, IL-6 and IL-10 were similar in BAL fluid of *Setdb2*$^{GT/GT}$ and WT mice (**Supplementary Fig. 8a-c**). Despite increased amounts of CXCL1 in *Setdb2*$^{GT/GT}$ mice upon influenza virus infection, both mouse strains showed comparable neutrophil infiltration in the lung at this stage of infection (**Fig. 5c, d**). A comprehensive profiling of other cell populations in the lung tissue and BAL, including monocytes, macrophages, dendritic cells, alveolar macrophages, NK cells, T cells and B cells revealed no differences in uninfected as well as in influenza virus infected *Setdb2*$^{GT/GT}$ and WT mice (**Supplementary Fig. 9a-d)**. The viral loads were comparable in both mouse strains (**Supplementary Fig. 10a**). In single infection with SP, *Setdb2*$^{GT/GT}$ and WT mice exhibited no significant differences in the induction of CXCL1 (**Supplementary Fig. 8d**), the numbers of neutrophils (**Supplementary Fig. 9e, f**) or the bacterial burden (**Supplementary Fig. 10b**).

Superinfection of influenza virus-infected mice with SP led to a further increase of CXCL1 (**Fig. 5b**). This was accompanied by increased infiltration of neutrophils in lung tissue and in the BAL fluid of *Setdb2*$^{GT/GT}$ but not WT mice (**Fig. 5c, d, Supplementary Fig. 9g, h**). Two days after superinfection with SP, mice showed severe signs of pneumonia (**Fig. 5e**) and pulmonary edema as measured by lung wet weight (**Fig. 5f**). The gross pathological appearance including size, weight, number of affected lobes, and hemorrhagic lesions of *Setdb2*$^{GT/GT}$ lungs was milder as compared to WT controls (**Fig. 5e, f**). Histopathological analysis of lung sections confirmed and extended the macroscopic findings, showing reduced signs of pneumonia including bronchitis, endothelialitis and inflammatory infiltrates (**Fig. 5g, h**). In line with the ameliorated pathological findings in *Setdb2*$^{GT/GT}$ mice at this advanced stage of bacterial superinfection, we found decreased levels of mRNA and protein of the pro-inflammatory cytokine IL-6 (**Fig. 5i, j**) and a reduced bacterial burden compared to WT control (**Fig. 5k**). Taken together, these data indicate that influenza virus-induced Setdb2 expression had a detrimental effect on the early recruitment of neutrophils, the subsequently delayed pathogen clearance and the impaired tissue integrity during bacterial superinfection.

DISCUSSION

Maintaining a balance between effective pathogen defense and the prevention of excessive inflammation, autoimmunity, and immunopathology is the central task of immune regulation [10, 12]. Type I IFN and NF-κB signaling are two important pathways for this process and are subjected to multiple layers of crosstalk, many of which are still poorly

understood. In particular, chromatin modifiers are increasingly recognized as crucial mediators and effectors of immune regulatory mechanisms.

We identified Setdb2 as a crucial part of the IFN-mediated immune response that provides a hitherto unknown layer of regulatory crosstalk between the type I IFN and NF-κB signaling pathways. The Setdb2-related SUV39 family members Suv39H1, Ehmt1 (alias: Glp) and Ehmt2 (alias: G9a) were shown to be involved in immunological processes such as the modulation of ISG expression, the NF-κB pathway and T cell differentiation [17, 19, 32]. Our finding of Setdb2 being an ISG itself points towards an important role in the innate immune response, which may contribute to the prevention of excessive immune-mediated pathology in particular infections and/or inflammatory conditions. Notably, single nucleotide polymorphisms in human *SETDB2* were shown to be associated with increased IgE production and atopic asthma [33], highlighting the proposed role of Setdb2 in regulating inflammation. This evolutionary strategy, however, may turn into a double-edged sword during bacterial superinfection, by causing impaired bacterial clearance and severe tissue damage. Previously, type I IFN signaling was shown to have a detrimental role in the pathogenesis of virus-induced susceptibility to bacterial superinfection [4, 13, 14, 15]. Accordingly, Setdb2 may be responsible and mediate at least parts of this important type I IFN-dependent mechanism.

Chromatin modifiers can be recruited to their targets through specific interactions with transcriptional regulators and/or chromatin-associated factors. We hypothesize that a similar mechanism facilitates the specific recruitment of Setdb2 to its target gene promoters to introduce repressive H3K9me3 chromatin marks. Yet, we cannot exclude the possibility that Setdb2 may recruit other methyltransferases or transcription factors. Likewise, the function of Setdb2 may be determined by mutually non-exclusive cellular and immunological parameters (e.g. cell type, inflammatory state, pathogen type) as well as by the complex epigenetic context of multivalent chromatin modifications [34]. Independent of direct histone methylation and in analogy to other PKMTs, Setdb2 may also methylate non-histone protein targets [32, 35].

This study shows that reduced amounts of Setdb2 lead to increased production and secretion of CXCL1. Our data suggest that the increased CXCL1 expression and neutrophil recruitment observed in *Setdb2*$^{GT/GT}$ mice may be causally involved in the ameliorated pathogenesis of bacterial superinfection. Neutrophils execute multiple roles including the regulation and resolution of inflammation and the elimination of bacterial pathogens [29, 36]. In this study we observed increased CXCL1 expression in the lungs of influenza virus infected *Setdb2*$^{GT/GT}$ compared to WT mice. This alteration in chemokine production and secretion was not sufficient to augment the virus-induced neutrophil response. The increased CXCL1 expression in *Setdb2*$^{GT/GT}$ mice manifested phenotypically only upon superinfection as elevated numbers of neutrophils in the lungs. This could be due to altered time kinetics of the host response and/or the involvement of additional signals provided by the bacterial superinfection. Together, our data suggest that the influenza virus-induced expression of Setdb2 reduced the antibacterial response in WT mice, leading to aggravated lung pathology.

These findings provide evidence for a regulatory function of Setdb2 in CXCL1 expression, the recruitment of neutrophils, and the pathological outcome of superinfections. However, we cannot exclude that other Setdb2-modulated genes may contribute to improved bacterial clearance and reduced tissue inflammation in *Setdb2*$^{GT/GT}$ mice. Our RNAseq experiment performed with poly(I:C) stimulation identified several other upregulated antibacterial genes in *Setdb2*$^{GT/GT}$ BMDMs. These genes included the chemotactic proteins S100a8/9 [37], Marco, a macrophage scavenger receptor that is implicated in the phagocytosis and clearance of bacteria in the lung [38], as well as Chi3l1, which was demonstrated to promote both improved clearance of SP and disease tolerance [39]. Yet, their expression profiling by real-time PCR revealed no differences between superinfected WT and *Setdb2*$^{GT/GT}$ mice under the experimental conditions of this study (data not shown). Finally, Setdb2 may not only regulate antibacterial responses but may as well modulate genes involved in disease tolerance in superinfection [40].

In summary, our study assigns Setdb2 an important regulatory role in the IFN-mediated immune response and in the pathogenesis of virus-induced susceptibility to bacterial superinfection. Several inhibitors for PKMTs are currently in clinical trials [41]. Thus, Setdb2 could be an attractive therapeutic target for the treatment of superinfections and other inflammatory conditions.

ONLINE METHODS

Mice

C57BL/6J mice (WT) were obtained from The Jackson Laboratory and *Ifnar1*$^{-/-}$ [42], *Irf7*$^{-/-}$ [43], *Stat1*$^{-/-}$ [44] and *Tlr2*$^{-/-}$*Cd36*$^{-/-}$ [45, 46] mice were on a C57BL/6J background. To generate Setdb2$^{GT/GT}$ mice, the targeting vector pEKF106 was made by recombineering using Lambda RED system in *E. coli* strain EL350 [47]. A genomic PAC library (i.e. from the 129/SvevTACfBr genetic background, RPCI mouse PAC library 21; MRC Geneservice) was screened for the full-length *Setdb2* gene using specific cDNA probes. A positive PAC clone, RP21-498J23, was used for recovery of flanking genomic sequences. We generated a 2.3kb genomic fragment introducing an EcoRV restriction site and loxP-*Neo* using plasmid pLMJ237, for insertion downstream of exon 3. *Neo* was removed by arabinose induction of Cre recombinase. Similarly, a 2.9kb genomic fragment harboring the frt-loxP flanked gene trap cassette and a heterologous BamHI restriction site was generated by recombineering using pLTM330. The gene trap cassette contains a pGK/EM7 dual promoter, a strong splice acceptor site from the *engrailed 2* gene, and *Neo* reporter gene, followed by a strong polyadenylation signal (**Supplementary Fig. 3A**). NotI linearized targeting vector DNA was transfected into v6.4 embryonic stem (ES) cells, a hybrid of the C57BL/6J × 129/SvJae lineages. Transfected ES cells were selected for neomycin resistance with G418 and positive clones were tested by Southern blot analysis of EcoRV-digested DNA (**Supplementary Fig. 3B**). Positive ES cell clones were microinjected into blastulae and transferred to pseudopregnant female mice, following standard methods. Mice were genotyped for the presence of the gene trap cassette by Southern blot hybridization (not shown) and by PCR amplification of genomic DNA using primers 5'-AATGGGCCATATTAGTAGAAGC-3' and 5'-GATCTTGCTCAAAGGTCACCA-3' (**Supplementary Fig. 3C**). The WT allele

amplicon was a 422 bp PCR product, while the knocked-in gene trap amplicon was a 516 bp PCR product. All Setdb2$^{GT/GT}$ mice used in this study were backcrossed for >10 generations onto a C57BL/6J background.

All mice were kept under specific pathogen-free conditions at the Institute of Molecular Biotechnology (IMBA) of the Austrian Academy of Sciences, the Medical University of Vienna, National Cancer institute, the Ohio State University, and/or the Institute for Systems Biology, Seattle. For all experiments sex- and age-matched mice were used. The animal protocols were approved by the Institutional Animal Care and Use Committees of the National Cancer Institute-Frederick, the Ohio State University, the Institute of Systems Biology in Seattle respectively by the ethical committee of the Medical University of Vienna and the Austrian Federal Ministry of Science and Research.

Bone marrow-derived macrophages

Bone marrow-derived macrophages (BMDMs) were isolated from C57BL/6J, *Ifnar1*$^{-/-}$ and *Setdb2*$^{GT/GT}$ mice and cultured in RPMI medium containing 10% FBS, penicillin-streptomycin-glutamine (Life Tech #10378-016) and 50ng/ml recombinant mouse macrophage colony stimulating factor (eBioscience #34-8983-85). BMDMs were stimulated with PAM3CSK4 (PAM3) (500ng/ml, Invivogen tlrl-pms), poly(I:C) (6μg/ml, Invivogen tlrl-pic), LPS (20ng/ml, *Salmonella enterica* serotype Minnesota, Sigma #L4641), mouse IFNβ (1000 IU/ml, PBL Interferon Source #12400-1), mouse IFNγ (100ng/ml, Peprotech #315-05) or IFNλ2 (100ng/ml, Biomedica 4635-ML-025). For *in vitro* infections with influenza virus A/PR/8/34, cells were grown in OPTI-MEM medium (Life Tech, #31985-070) containing 4% BSA (Sigma, #A7979), 1x MEM vitamins solution (Life Tech, #11120-037) and 1μg/ml TPCK trypsin (Sigma, #T8802). To block IFNAR1, we pre-treated BMDMs with 20μg/ml of IFNAR1-specific antibody (clone MAR1-5A3, BioXCell #BE0241) [48] or with mouse IgG1 isotype control (clone MOPC-21, BioXCell #BE0083) 18 hours prior to poly(I:C) stimulation and added fresh antibody upon stimulation.

Microarray analysis

Total RNA was extracted with Trizol (Life Technologies) and RNA quality was determined by Bioanalyzer (Agilent). For the experiments shown in **Fig. 1a-c** and **Supplementary Table 1**, RNA was processed for hybridization to GeneChip Mouse Exon 1.0 ST arrays according to the manufacturer`s instructions (Affymetrix). Exon-level signal values were generated by Affymetrix Power Tools. The Institute of Systems Biology`s GenePattern Exon pipeline was used to generate transcript-level expression values. PERL scripts were used to combine and annotate these data. For the experiments shown in **Supplementary Fig. 2** and **Supplementary Table 3**, publicly available array expression data derived from poly(I:C) stimulated BMDMs was downloaded from the website http://www.systemsimmunology.org.

RNA sequencing

For the experiments in **Fig. 2b** and **Supplementary Table 4**, we performed expression analysis by RNAseq. Briefly, BMDMs from each genotype were prepared and stimulated with poly(I:C) for the indicated time points. RNA was extracted by QIAzol lysis reagent

(Qiagen) and the libraries were prepared with the Truseq RNA sample preparation kit v2 according to the manufacturer`s instructions (Illumina). Quality control analysis was performed by Experion DNA Analysis chip (Biorad) and Qubit Fluorometric Quantitation (Life Technologies). The samples were multiplexed with 9 samples per lane and run on a 50bp single-end flow cell in a Hiseq2000 sequencer (Illumina). RNA-Seq reads were aligned to the mouse genome assembly GRCm38 (UCSC mm10) with the TopHat splice junction mapper (version 2.0.12) utilizing the mouse gene and transcript annotation from Ensembl version 70 as reference transcriptome. The TopHat max-multihits option were set to 100, while the length (-L) of the seed substrings of the underlying Bowtie 2 aligner (version 2. 2.3) were reduced from 20 to 15. Programs from the Cufflinks package (version 2. 2.1) were used to assemble transcripts, merge transcript assemblies of replicates and samples before finally testing for differential expression with the Cuffdiff program. The default false discovery rate (FDR) of 0.05 was left unchanged. Cuffdiff comparisons were post-processed, and quality assessment plots were drawn with the Bioconductor package cummeRbund (version 2.6.1).

Bioinformatics analyses

Gene ontology enrichment analyses were done by DAVID Bioinformatics Resources 6.7 and the Molecular Signatures Database of Gene Set Enrichment Analysis (GSEA). Enrichment analysis of transcription factor binding targets was performed by GSEA using transcription factor binding sites as defined in TRANSFAC version 7.4. The computed Robust Multi-array Average (RMA) values were subjected to Significance Analysis of Microanalysis (SAM) using Microarray expression Viewer v4.9. A two-class paired test with default parameters was used and calculated the *Delta* and a cutoff of 3 to compute the significantly regulated genes. Heatmaps were plotted in R. The motif scanning for transcription factor binding sites was performed +/− 3kb up- and downstream of the transcriptional start site of Setdb2 as described previously [11].

A list of NF-κB target genes was compiled using resources from the website of The Gilmore Lab, Boston University (http://www.bu.edu/nf-kb/gene-resources/target-genes/), from the website of the Institut de Biologie de Lille et LIFL (http://bioinfo.lifl.fr/NF-KB/#haut%20de%20page) as well as from recent literature. The resulting total list of 373 NF-κB target genes (**Supplementary Table 5**) was used to calculate the hypergeometric distribution (assuming a total number of 24561 coding genes, source: MGI informatics.jax.org) of overlapping genes within the protein-coding genes that were significantly upregulated > 1.5-fold at ≥ one time point ($p<0.001$).

Real-time PCR—For the measurement of gene expression by real-time PCR, total RNA was isolated using QIAzol lysis reagent (Qiagen) and reverse-transcribed with the First Strand cDNA Synthesis Kit (Fermentas). Subsequently gene expression was analyzed using Taqman Fast Universal PCR Mastermix and Taqman Gene Expression assays (*Setdb2*: Mm01318748_m1, *Cxcl1*: Mm00433859_m1, *Il6*: Mm00446190_m1) (Life Technologies) as well as an assay for the M gene of influenza virus A/PR/8/34 using the oligonucleotides F 5’- CATGGAATGGCTAAAGACAAGACC-3’, R 5’-CCATTAAGGGCATTTTGGACA-3` and taqman probe 5’-FAM-

TTTGTGTTCACGCTCACCGTGCCCA-BHQ1-3'. Real-time PCR experiments were run on a 7900HT Real-Time PCR system or a StepOnePlus Real-Time PCR system (Life Technologies). Expression data was normalized to the housekeeping gene *Eef1a1* (encoding eukaryotic translation elongation factor 1 α1). Fold-induction was calculated by comparison to the untreated WT control group.

Generation of a Setdb2-specific monoclonal antibody—A C-terminal 60 amino acid long sequence (amino acid position 541-600) was fused into a hepatitis B carrier protein as immunogen. This region was amplified by PCR and inserted into a 6x histidine-tagged pB-His HBcAg_Linker plasmid [49]. The fusion protein was expressed in *E. coli* BL21 and purified on 1ml HisTrap HP columns (GE Healthcare) followed by a linear imidazole gradient on an ÄKTA FPLC system (GE Healthcare). The fractions were analyzed by SDS-Page and concentrated with Amicon Ultra 15-3K Centrifugal Filter Devices (Millipore). The immunization and generation of monoclonal B-cell hybridomas was performed by challenging *Setdb2*$^{GT/GT}$ mice 3 times (every 2 weeks) with 50μg of purified fusion protein antigen mixed 1:1 with adjuvant subcutaneously, before a final immunization intravenously with 50μg purified antigen (adjuvant-free). Mouse sera and clone pools were tested by western blot against overexpressed and endogenous mouse Setdb2. Clone 7H7F11 yielded the best signal-to-noise performance.

Immunoblot—Protein concentration of cell lysates and organs were determined with a Coomassie Protein Assay kit (Thermo Scientific). Proteins were analyzed by SDS-Page using NuPAGE® Novex 4-12% Bis-Tris Gels (Life Technologies), Westran® Clear signal PVDF membranes (Whatman) and the following antibodies: anti-Zbp1 (kindly provided by the Superti-Furga laboratory), anti-Setdb2 (clone 7H7F11, described in this study), anti-IκBα (Santa Cruz Biotechnology sc-371 clone C-21, respectively, Cell Signaling n.4814 clone L35A5) and anti-actin (Sigma #A2066). The protein size was determined with the PageRuler™ Prestained Protein Ladder (Thermo Scientific). Detection was done with Pierce ECL Western blotting substrate (Thermo Scientific) or Amersham ECL select Western blotting detection reagent (GE Healthcare Life Sciences). Gels were visualized with the chemiluminescent gel documentation system F-ChemiBIS 3.2 (DNR Bio-Imaging Systems).

ELISA—Protein concentrations were determined using the Mouse CXCL1/KC Quantikine ELISA Kit (#MKC00B) or the Mouse CXCL1/KC DuoSet (#DY453), the Mouse CXCL2/MIP-2 DuoSet (#DY452), the Mouse IL-6 DuoSet (#DY406) (R&D Systems) or the Mouse BD OptEIA IL-10 kit (BD Biosciences, #555252). The ELISAs were performed according to the manufacturer`s instructions.

Chromatin immunoprecipitation analysis—BMDMs derived from WT or *Setdb2*$^{GT/GT}$ mice were either treated with poly(I:C) for 2h or left untreated. The same number of cells was subsequently harvested, fixed with 1% formaldehyde for 10min at RT, and lysed in 1% SDS buffer. Chromatin was sheared to an average size of 300bp using S2X Focused-ultrasonicator (Covaris), and the amount was adjusted using ND-1000 spectrophotometer (NanoDrop) measurement to match WT and *Setdb2*$^{GT/GT}$ samples before histone mark ChIPs. The prepared chromatin of WT or WT and *Setdb2* $^{GT/GT}$ samples were

subjected to ChIP with anti-Setdb2 clone 7H7F11 (see above), anti-H3K9me3 (Abcam Ab8898) or anti-H3K9acetyl (Millipore #07-352) respectively following a procedure as described previously [50] that was modified by the use of magnetic Dynabeads Protein-G beads (Life Technologies). For mock ChIP controls, empty beads were used. For mock controls in Setdb2 ChIP, the medium used for culturing the hybridoma 7H7F11 was added instead. The ChIP efficiency was controlled by quantitative real-time PCR analysis using the primers for: *Cxcl1* promoter region, F 5'-CCTCTTCACATGCCTCCCTG-3' and R 5'-CGGGGATGGAAGCTTGTCTT-3'; *Cxcl1* exon 1 region, F 5'-GTTCCAGCACTCCAGACTCC-3' and R 5'-AGTGGCGAGACCTACCTGT-3'; *Actb* promoter region, F 5'-CCTCTGGGTGTGGATGTCAC-3' and R 5'-TGTCCATTCAATCCAGGCCC-3'.

LPS-induced pulmonary neutrophilia model—Mice were anesthetized with ketamine/xylazine and intranasally administered with 0.4 μg of LPS (*E. coli* serotype 0111:B4, Sigma #L4391) as described previously. Four hours later, mice were sacrificed and bronchoalveolar lavage (BAL) was taken by washing the lungs 3 times with PBS in a total volume of 1 ml. The total number of cells in the BAL fluid was enumerated with an improved Neubauer hemocytometer. Cytocentrifuged preparations (Cytospin-4, Shandon Instruments) were stained with Kwik-Diff Stains (Thermo Fisher Scientific) and the percentage of inflammatory cells was determined by morphological examination of at least 300 cells per sample.

Infection models—For the lung analyses in **Fig. 1**, mice were anesthetized with ketamine/xylazine and intranasally infected with 15μl or 50μl of PBS containing ~10^5 plaque forming units (PFU) of influenza virus A/PR/8/34 (PR8) (originally obtained from Charles River Laboratories). In all other experiments mice were infected intranasally with a sublethal dose of PR8 (~10^2 PFU) or the indicated dose of *Streptococcus pneumoniae* (SP) strain ATCC 6303. Mice for the 16h samples in **Fig. 5** were harvested in the time span corresponding to 14-16h after superinfection. Bacterial titers were determined from lung homogenates by plating 10-fold serial dilutions on blood agar plates. The lung wet weights were determined with a Pioneer precision balance (Ohaus).

Flow cytometric analysis—Lung tissue was harvested as indicated and single cell suspension were prepared using a metal mesh. Absolute cell numbers were counted with a Neubauer chamber. Single-cell suspensions of the lungs respectively collected BAL fluid cells were incubated with CD16/CD32 Fc block (clone 93, BioLegend, 101310) to inhibit unspecific antibody binding. For flow cytometry, cells were stained with the following antibodies: anti-B220/CD45R (clone RA3-6B2, eBioscience, 45-0452), anti-CD3ε (clone 145-2C11, BioLegend, 100320), anti-CD11b (clone M1/70, BioLegend, 101206), anti-Ly-6G (clone 1A8, eBioscience, 17-9668), anti-CD45 (clone 30-F11, BioLegend, 103137), anti-CD11c (clone N418, Biolegend, 117333) and anti-SiglecF (clone E50-2440, BD, 562681). To exclude dead cells from the analysis, the samples were labeled with the Fixable Viability Dye eFluor 780 (eBioscience, 65-0865).

Histology—Lung tissue was fixed with either 4% paraformaldehyde or 10% formalin and embedded in paraffin. Immunohistochemistry was performed on 3-4 μm thick sections. Endogenous peroxidase was neutralized (PBS/3% H2O2) and unspecific binding blocked (PBS/10% FCS). Sections were then incubated with goat-anti influenza antibody (Serotec, Product Code 5315-0064) overnight at 4°C. Bound primary antibody was visualized by a biotin technique with 3,3' diaminobenzidine as chromogen (haemalaun counterstaining of nuclei).

In **Fig. 5h**, histology scores were obtained by a trained pathologist, blinded for groups, from lung sections stained with hematoxylin and eosin [59]. The severity of inflammation and pneumonia was evaluated based on the presence of interstitial inflammation, alveolar inflammation, pleuritis, bronchitis and endothelitis with 0 representing absent, 1 mild, 2 moderate, and 3 severe. Additionally, 1 point was added for the presence of pneumonia, edema or thrombi formation, and 0.5 point for every infiltrate covering 10% of the lung area. The sum of all parameters indicates the total histology score.

Statistical Analysis—Results are indicated as line graph, bar graph or scatter plot with the mean +/− standard error of the mean as indicated. Statistical differences between experimental groups were determined by unpaired t-test as detailed in the figure legends. If variances (F-test) between the compared data sets were significantly different, an unpaired t-test with Welch's correction was performed. Significant p-values were indicated as follows: * $p \leq 0.05$, ** $p \leq 0.01$, *** $p \leq 0.001$, **** $p \leq 0.0001$. Graphs and statistical tests were done with GraphPad Prism version 5 and 6.

Supplementary Material

Refer to Web version on PubMed Central for supplementary material.

Acknowledgements

We would like to thank Stefan Schüchner and Egon Ogris from the Max F. Perutz Laboratories Monoclonal antibody facility in Vienna, Eileen Southon and Mary Ellen Palko from the Mouse Cancer genetics Program, National Cancer Institute, Yingshi Guo of the Ohio State University, Bruz Marzolf and Pamela Troisch from the microarray core facility of the Institute for Systems Biology, Matthias Farlik, Thomas Penz, Michael Schuster and Christoph Bock from the Biosequencing Facility of CeMM, and Mathias Müller and Birgit Strobl for provision of mice. We would also like to acknowledge advice and/or sharing of reagents by Maria Gorna, Florian Grebien, Leonhard Heinz, Thomas Karonitsch, Manuele Rebsamen, Carrie Rosenberger and Simona Saluzzo.

We thank Denise Barlow, Richard A. Flavell, Ahmed N. Hegazy, Amanda Jamieson, Ruslan Medzhitov and Giulio Superti-Furga for valuable discussions and input.

C.S. was supported by a fellowship within the Postdoc-Program of the German Academic Exchange Service (DAAD). E.K.F., A.L.T., L.T. and D.E.S. were supported by the Intramural Research Program of the NCI, Center for Cancer Research, NIH. R.K.K. is supported by an European Molecular Biology Organization (EMBO) long-term fellowship (ALTF 314-2012). A.Bh. is supported by a DOC fellowship of the Austrian Academy of Sciences. D.M. holds stipendiary professorships of the Swiss National Science Foundation (No. PP00P3_152928) and is supported by the Klaus-Tschira Foundation and Gebert-Rüf Foundation. D.E.S. was supported by startup funds from the Ohio State University Comprehensive Cancer Center. This work was supported by grants R01AI032972, R01AI025032 and U19AI100627 from the National Institutes of Health (A.A.). A.B. was a long-term EMBO fellow and recipient of a Fellowship for Advanced Researchers from the Swiss Foundation for Medical-Biological Stipends (SSMBS), and was supported by the Austrian Academy of Sciences and grant number 25360 of the Austrian Science Foundation (FWF).

References

1. Morens DM, Taubenberger JK, Fauci AS. Predominant role of bacterial pneumonia as a cause of death in pandemic influenza: implications for pandemic influenza preparedness. The Journal of infectious diseases. 2008; 198(7):962–970. [PubMed: 18710327]
2. Molinari NA, Ortega-Sanchez IR, Messonnier ML, Thompson WW, Wortley PM, Weintraub E, et al. The annual impact of seasonal influenza in the US: measuring disease burden and costs. Vaccine. 2007; 25(27):5086–5096. [PubMed: 17544181]
3. van der Sluijs KF, van der Poll T, Lutter R, Juffermans NP, Schultz MJ. Bench-to-bedside review: bacterial pneumonia with influenza - pathogenesis and clinical implications. Critical care. 2010; 14(2):219. [PubMed: 20459593]
4. McCullers JA. The co-pathogenesis of influenza viruses with bacteria in the lung. Nature reviews Microbiology. 2014; 12(4):252–262. [PubMed: 24590244]
5. Kawai T, Akira S. The role of pattern-recognition receptors in innate immunity: update on Toll-like receptors. Nat Immunol. 2010; 11(5):373–384. [PubMed: 20404851]
6. Taniguchi T, Ogasawara K, Takaoka A, Tanaka N. IRF family of transcription factors as regulators of host defense. Annu Rev Immunol. 2001; 19:623–655. [PubMed: 11244049]
7. Sadler AJ, Williams BR. Interferon-inducible antiviral effectors. Nat Rev Immunol. 2008; 8(7):559–568. [PubMed: 18575461]
8. Schoggins JW, Macduff DA, Imanaka N, Gainey MD, Shrestha B, Eitson JL, et al. Pan-viral specificity of IFN-induced genes reveals new roles for cGAS in innate immunity. Nature. 2013
9. Oeckinghaus A, Ghosh S. The NF-kappaB family of transcription factors and its regulation. Cold Spring Harbor perspectives in biology. 2009; 1(4):a000034. [PubMed: 20066092]
10. Medzhitov R, Schneider DS, Soares MP. Disease tolerance as a defense strategy. Science. 2012; 335(6071):936–941. [PubMed: 22363001]
11. Litvak V, Ratushny AV, Lampano AE, Schmitz F, Huang AC, Raman A, et al. A FOXO3-IRF7 gene regulatory circuit limits inflammatory sequelae of antiviral responses. Nature. 2012; 490(7420):421–425. [PubMed: 22982991]
12. Rouse BT, Sehrawat S. Immunity and immunopathology to viruses: what decides the outcome? Nat Rev Immunol. 2010; 10(7):514–526. [PubMed: 20577268]
13. Navarini AA, Recher M, Lang KS, Georgiev P, Meury S, Bergthaler A, et al. Increased susceptibility to bacterial superinfection as a consequence of 25 innate antiviral responses. Proc Natl Acad Sci U S A. 2006; 103(42):15535–15539. [PubMed: 17030789]
14. Nakamura S, Davis KM, Weiser JN. Synergistic stimulation of type I interferons during influenza virus coinfection promotes Streptococcus pneumoniae colonization in mice. J Clin Invest. 2011; 121(9):3657–3665. [PubMed: 21841308]
15. Shahangian A, Chow EK, Tian X, Kang JR, Ghaffari A, Liu SY, et al. Type I IFNs mediate development of postinfluenza bacterial pneumonia in mice. J Clin Invest. 2009; 119(7):1910–1920. [PubMed: 19487810]
16. Foster SL, Hargreaves DC, Medzhitov R. Gene-specific control of inflammation by TLR-induced chromatin modifications. Nature. 2007; 447(7147):972–978. [PubMed: 17538624]
17. Fang TC, Schaefer U, Mecklenbrauker I, Stienen A, Dewell S, Chen MS, et al. Histone H3 lysine 9 di-methylation as an epigenetic signature of the interferon response. J Exp Med. 2012; 209(4): 661–669. [PubMed: 22412156]
18. Satoh T, Takeuchi O, Vandenbon A, Yasuda K, Tanaka Y, Kumagai Y, et al. The Jmjd3-Irf4 axis regulates M2 macrophage polarization and host responses against helminth infection. Nat Immunol. 2010; 11(10):936–944. [PubMed: 20729857]
19. Allan RS, Zueva E, Cammas F, Schreiber HA, Masson V, Belz GT, et al. An epigenetic silencing pathway controlling T helper 2 cell lineage commitment. Nature. 2012; 487(7406):249–253. [PubMed: 22763435]
20. Dillon SC, Zhang X, Trievel RC, Cheng X. The SET-domain protein superfamily: protein lysine methyltransferases. Genome Biol. 2005; 6(8):227. [PubMed: 16086857]

21. Matsui T, Leung D, Miyashita H, Maksakova IA, Miyachi H, Kimura H, et al. Proviral silencing in embryonic stem cells requires the histone methyltransferase ESET. Nature. 2010; 464(7290):927–931. [PubMed: 20164836]
22. Ceol CJ, Houvras Y, Jane-Valbuena J, Bilodeau S, Orlando DA, Battisti V, et al. The histone methyltransferase SETDB1 is recurrently amplified in melanoma and accelerates its onset. Nature. 2011; 471(7339):513–517. [PubMed: 21430779]
23. Xu PF, Zhu KY, Jin Y, Chen Y, Sun XJ, Deng M, et al. Setdb2 restricts dorsal organizer territory and regulates left-right asymmetry through suppressing fgf8 activity. Proc Natl Acad Sci U S A. 2010; 107(6):2521–2526. [PubMed: 20133783]
24. Falandry C, Fourel G, Galy V, Ristriani T, Horard B, Bensimon E, et al. CLLD8/KMT1F is a lysine methyltransferase that is important for chromosome segregation. J Biol Chem. 2010; 285(26):20234–20241. [PubMed: 20404330]
25. Hogarth CA, Mitchell D, Evanoff R, Small C, Griswold M. Identification and expression of potential regulators of the mammalian mitotic-to-meiotic transition. Biol Reprod. 2011; 84(1):34–42. [PubMed: 20826732]
26. Richon VM, Johnston D, Sneeringer CJ, Jin L, Majer CR, Elliston K, et al. Chemogenetic analysis of human protein methyltransferases. Chem Biol Drug Des. 2011; 78(2):199–210. [PubMed: 21564555]
27. Takaoka A, Mitani Y, Suemori H, Sato M, Yokochi T, Noguchi S, et al. Cross talk between interferon-gamma and -alpha/beta signaling components in caveolar membrane domains. Science. 2000; 288(5475):2357–2360. [PubMed: 10875919]
28. Black JC, Van Rechem C, Whetstine JR. Histone lysine methylation dynamics: establishment, regulation, and biological impact. Mol Cell. 2012; 48(4):491–507. [PubMed: 23200123]
29. Mantovani A, Cassatella MA, Costantini C, Jaillon S. Neutrophils in the activation and regulation of innate and adaptive immunity. Nat Rev Immunol. 2011; 11(8):519–531. [PubMed: 21785456]
30. McNamee LA, Harmsen AG. Both influenza-induced neutrophil dysfunction and neutrophil-independent mechanisms contribute to increased susceptibility to a secondary Streptococcus pneumoniae infection. Infect Immun. 2006; 74(12):6707–6721. [PubMed: 16982840]
31. Cai S, Batra S, Lira SA, Kolls JK, Jeyaseelan S. CXCL1 regulates pulmonary host defense to Klebsiella Infection via CXCL2, CXCL5, NF-kappaB, and MAPKs. J Immunol. 2010; 185(10): 6214–6225. [PubMed: 20937845]
32. Levy D, Kuo AJ, Chang Y, Schaefer U, Kitson C, Cheung P, et al. Lysine methylation of the NF-kappaB subunit RelA by SETD6 couples activity of the histone methyltransferase GLP at chromatin to tonic repression of NF-kappaB signaling. Nat Immunol. 2011; 12(1):29–36. [PubMed: 21131967]
33. Zhang Y, Leaves NI, Anderson GG, Ponting CP, Broxholme J, Holt R, et al. Positional cloning of a quantitative trait locus on chromosome 13q14 that influences immunoglobulin E levels and asthma. Nat Genet. 2003; 34(2):181–186. [PubMed: 12754510]
34. Ruthenburg AJ, Li H, Patel DJ, Allis CD. Multivalent engagement of chromatin modifications by linked binding modules. Nat Rev Mol Cell Biol. 2007; 8(12):983–994. [PubMed: 18037899]
35. Marazzi I, Ho JS, Kim J, Manicassamy B, Dewell S, Albrecht RA, et al. Suppression of the antiviral response by an influenza histone mimic. Nature. 2012; 483(7390):428–433. [PubMed: 22419161]
36. Nauseef WM, Borregaard N. Neutrophils at work. Nat Immunol. 2014; 15(7):602–611. [PubMed: 24940954]
37. Raquil MA, Anceriz N, Rouleau P, Tessier PA. Blockade of antimicrobial proteins S100A8 and S100A9 inhibits phagocyte migration to the alveoli in streptococcal pneumonia. J Immunol. 2008; 180(5):3366–3374. [PubMed: 18292562]
38. Arredouani M, Yang Z, Ning Y, Qin G, Soininen R, Tryggvason K, et al. The scavenger receptor MARCO is required for lung defense against pneumococcal pneumonia and inhaled particles. J Exp Med. 2004; 200(2):267–272. [PubMed: 15263032]
39. Dela Cruz CS, Liu W, He CH, Jacoby A, Gornitzky A, Ma B, et al. Chitinase 3-like-1 promotes Streptococcus pneumoniae killing and augments host tolerance to lung antibacterial responses. Cell host & microbe. 2012; 12(1):34–46. [PubMed: 22817986]

40. Jamieson AM, Pasman L, Yu S, Gamradt P, Homer RJ, Decker T, et al. Role of tissue protection in lethal respiratory viral-bacterial coinfection. Science. 2013; 340(6137):1230–1234. [PubMed: 23618765]

41. Helin K, Dhanak D. Chromatin proteins and modifications as drug targets. Nature. 2013; 502(7472):480–488. [PubMed: 24153301]

42. Muller U, Steinhoff U, Reis LF, Hemmi S, Pavlovic J, Zinkernagel RM, et al. Functional role of type I and type II interferons in antiviral defense. Science. 1994; 264(5167):1918–1921. [PubMed: 8009221]

43. Honda K, Yanai H, Negishi H, Asagiri M, Sato M, Mizutani T, et al. IRF-7 is the master regulator of type-I interferon-dependent immune responses. Nature. 2005; 434(7034):772–777. [PubMed: 15800576]

44. Durbin JE, Hackenmiller R, Simon MC, Levy DE. Targeted disruption of the mouse Stat1 gene results in compromised innate immunity to viral disease. Cell. 1996; 84(3):443–450. [PubMed: 8608598]

45. Takeuchi O, Hoshino K, Kawai T, Sanjo H, Takada H, Ogawa T, et al. Differential roles of TLR2 and TLR4 in recognition of gram-negative and gram-positive bacterial cell wall components. Immunity. 1999; 11(4):443–451. [PubMed: 10549626]

46. Febbraio M, Podrez EA, Smith JD, Hajjar DP, Hazen SL, Hoff HF, et al. Targeted disruption of the class B scavenger receptor CD36 protects against atherosclerotic lesion development in mice. J Clin Invest. 2000; 105(8):1049–1056. [PubMed: 10772649]

47. Lee EC, Yu D, Martinez de Velasco J, Tessarollo L, Swing DA, Court DL, et al. A highly efficient Escherichia coli-based chromosome engineering system adapted for recombinogenic targeting and subcloning of BAC DNA. Genomics. 2001; 73(1):56–65. [PubMed: 11352566]

48. Sheehan KC, Lai KS, Dunn GP, Bruce AT, Diamond MS, Heutel JD, et al. Blocking monoclonal antibodies specific for mouse IFN-alpha/beta receptor subunit 1 (IFNAR-1) from mice immunized by in vivo hydrodynamic transfection. J Interferon Cytokine Res. 2006; 26(11):804–819. [PubMed: 17115899]

49. Kratz PA, Bottcher B, Nassal M. Native display of complete foreign protein domains on the surface of hepatitis B virus capsids. Proc Natl Acad Sci U S A. 1999; 96(5):1915–1920. [PubMed: 10051569]

50. Schebesta A, McManus S, Salvagiotto G, Delogu A, Busslinger GA, Busslinger M. Transcription factor Pax5 activates the chromatin of key genes involved in B cell signaling, adhesion, migration, and immune function. Immunity. 2007; 27(1):49–63. [PubMed: 17658281]

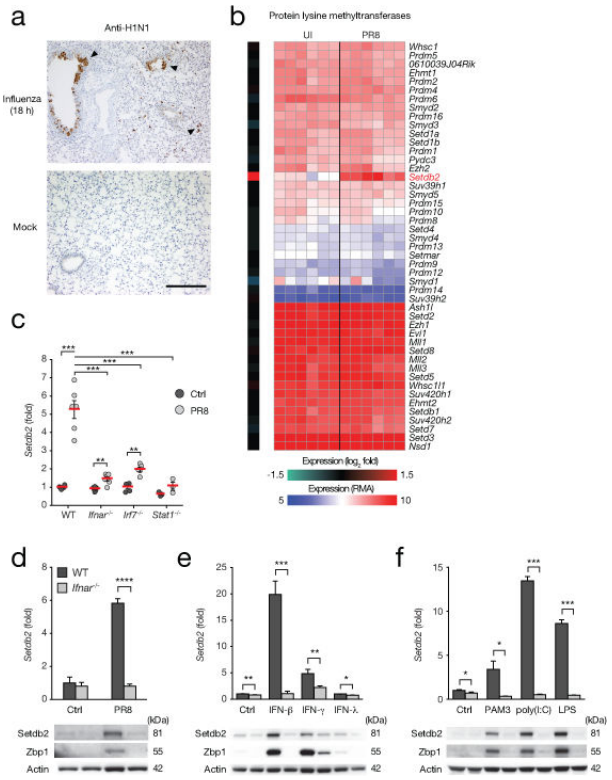

Figure 1.

Setdb2 is induced upon influenza virus infection and TLR stimulation in an IFNAR1 dependent manner. (**a**) WT mice were intranasally infected with influenza virus or mock treated. 18 hours later lung sections were stained using an H1N1-specific antibody. H1N1 infected areas are indicated by arrowheads. Scale bar, 250μm. Representative images for 3 individual mice are shown. (**b**) Expression profile of protein lysine methyltransferases (PKMTs) in lungs upon influenza virus infection (PR8) compared to uninfected controls (UI) (n=6, 2 experiments independent pooled). Heatmap illustrations of (left) log2-fold change compared to uninfected mice respectively (right) Robust Multi-array Average (RMA) values are shown. (**c**) WT, *Ifnar1*$^{-/-}$, *Irf7*$^{-/-}$ and *Stat1*$^{-/-}$ mice were intranasally infected with influenza virus (PR8) or mock treated (Ctrl). 18 hours later lung tissue was collected and expression of Setdb2 was determined by real-time PCR. Scatter blots represent the fold change of *Setdb2* expression of individual mice compared to uninfected WT mice. Data points were pooled from 2 independent experiments. (**d-f**) BMDMs from *Ifnar*$^{-/-}$ and WT mice were either left untreated (Ctrl), (**d**) infected with influenza virus (PR8, MOI 10), (**e**) stimulated with IFN-β, IFN-γ or IFN-λ, or (**f**) stimulated with the indicated TLR agonists PAM3, poly(I:C), and LPS. *Setdb2* mRNA expression was quantified by real-time PCR 8 hours after stimulation and is displayed as fold induction compared to untreated WT cells. Biological triplicates of one out of two similar independent experiments are shown. For protein detection, Setdb2 expression was analyzed (**d**) 8 hours respectively (**e, f**) 24 hours after stimulation by immunoblot using the Setdb2-specific mAb clone 7H7F11. Antibodies specific for the IFN-stimulated protein Zbp1 and actin served as controls for induction and loading, respectively. (**d, e**) Immunoblots show results of one out of two representative

experiments. (**c-f**) Statistical significance was calculated by unpaired t-test. Significant p-values were indicated as follows: * $p \leq 0.05$, ** $p \leq 0.01$, *** $p \leq 0.001$, **** $p \leq 0.0001$.

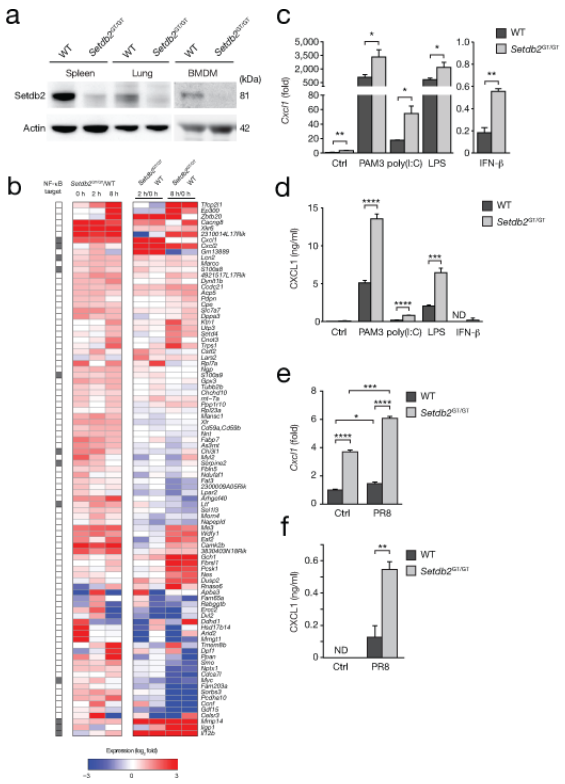

Figure 2.

Setdb2$^{GT/GT}$ macrophages show increased expression of a subset of NF-κB target genes including CXCL1. (**a**) Spleen and lung tissue as well as bone marrow-derived macrophages (BMDMs) from naive *Setdb2*$^{GT/GT}$ or WT mice were analyzed for the expression of Setdb2 by immunoblot using the Setdb2-specific mAb clone 7H7F11. Actin served as loading control. (**b**) BMDMs were treated with poly(I:C) for 0, 2 and 8 hours and expression profiling was performed by RNAseq using biological triplicates for each condition. Heatmap illustrations for (left) differential gene expression between WT and *Setdb2*$^{GT/GT}$ BMDMs of all protein-coding genes, respectively (right) the expression profiles at 2 and 8 hours compared to untreated BMDMs of the respective genotype are shown. NF-κB target genes are indicated as grey boxes. BMDMs from either WT or *Setdb2*$^{GT/GT}$ mice were either left untreated (Ctrl), (**c, d**) stimulated with the indicated TLR agonists and with IFN-β or (**e, f**) infected with influenza virus (PR8, MOI 10). (**c, e**) *Cxcl1* mRNA expression was quantified by real-time PCR after 2 hours of stimulation. (**d, f**) CXCL1 secretion was quantified by ELISA after 8 hours of stimulation. Biological triplicates of one out of two similar independent experiments are shown. (**c-f**) Statistical significance was calculated by unpaired t-test. Significant p-values were indicated as follows: * p≤0.05, ** p≤0.01, *** p≤0.001, **** p≤0.0001.

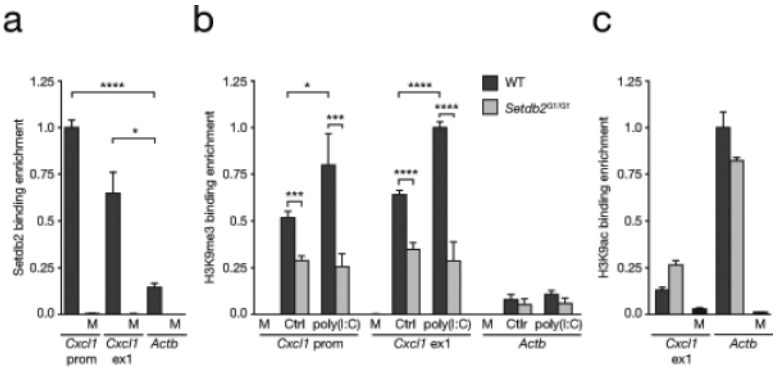

Figure 3.

Setdb2 binds to the *Cxcl1* promoter region and associates with H3K9 trimethylation. (**a-c**) WT or *Setdb2*$^{GT/GT}$ BMDMs were stimulated with poly(I:C) for 2 hours or left untreated (Ctrl) before cells were prepared for chromatin immunoprecipitation (ChIP). Specific enrichment of indicated promoter elements, the Cxcl1 promoter (prom) and the Cxcl1 exon 1 (ex1), was quantified by real-time PCR. Data are depicted as normalized recovery to the highest value in WT of duplicate measurements from two independent experiments (**a**, **b**), and one experiment (**c**). Empty beads from one respective experiment were used as mock (M). (**a**) ChIP for endogenous Setdb2 using the Setdb2-specific mAb clone 7H7F11. (**b**) ChIP for H3K9me3. (**c**) ChIP for H3K9ac. Statistical significance was calculated by unpaired t-test. Significant p-values were indicated as follows: * $p \leq 0.05$, ** $p \leq 0.01$, *** $p \leq 0.001$, **** $p \leq 0.0001$.

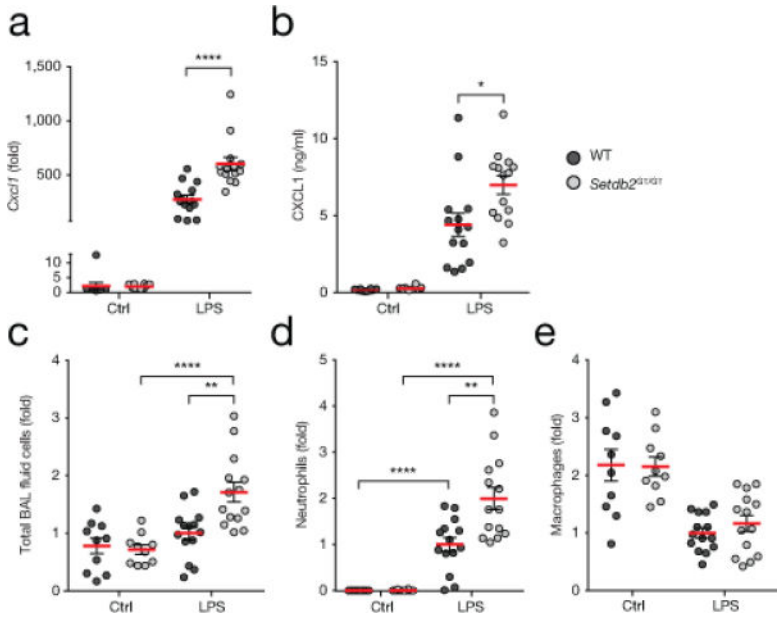

Figure 4.

Setdb2$^{GT/GT}$ mice show exacerbated lung inflammation in a model of LPS-induced neutrophilia. WT and *Setdb2*$^{GT/GT}$ mice were intranasally challenged with LPS for 4 hours or mock treated (Ctrl). (**a**) Total lung RNA from challenged and control mice was extracted and analyzed for the expression of *Cxcl1* by real-time PCR. (**b**) Bronchoalveolar lavage (BAL) was performed and BAL fluid supernatants were analyzed for CXCL1 by ELISA. (**c-e**), Total BAL fluid cells as well as neutrophils and macrophages were quantified. Cell numbers of individual experiments were normalized to the respective means of LPS-stimulated WT mice (relative number = cell number/mean$_{WT+LPS}$). Scatter blots represent individual mice pooled from 3 independent experiments. Statistical analysis was performed by unpaired t-test. Significant p-values were indicated as follows: * p≤0.05, ** p≤0.01, *** p≤0.001, **** p≤0.0001.

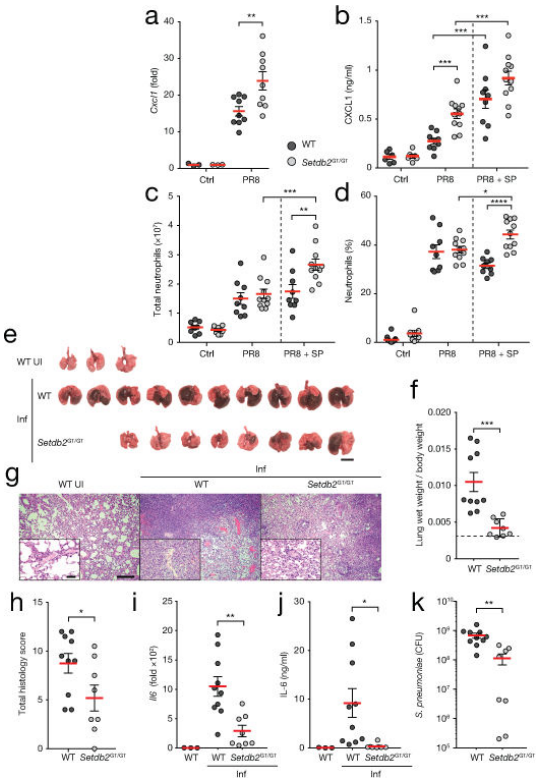

Figure 5.

Setdb2 mediates influenza virus-induced susceptibility to superinfection with *Streptococcus pneumoniae*. WT and *Setdb2*$^{GT/GT}$ mice were either left untreated (Ctrl), infected with a sublethal dose of influenza virus (PR8) or superinfected with *Streptococcus pneumoniae* (SP) 5 days after PR8 infection. (**a**) *Cxcl1* RNA was quantified by real-time PCR from lung tissue 5 days after influenza virus infection. (**b-d**) WT and *Setdb2*$^{GT/GT}$ mice were harvested 16 hours after SP superinfection. Superinfected mice received ~2×10^4 CFU of SP. (**b**) Results of CXCL1 ELISA from BAL fluid and enumeration of neutrophils from (**c**) lung tissue and (**d**) BAL fluid are shown. (**e-k**) 2 days after superinfection with ~2×10^3 CFU of SP, WT and *Setdb2*$^{GT/GT}$ mice were sacrificed and (**e**) images of lungs were taken (size bar, 1cm). Lungs were aligned according to the degree of gross pathology. (**f**) The lung wet weight was determined from the right lobes and normalized to the body weight on day zero. A dotted line depicts the average lung weight to body weight ratio of three uninfected lungs. (**g**) H&E histological staining of representative sections of the left lung lobes of WT and *Setdb2*$^{GT/GT}$ mice are shown. Scale bar of low magnification is 200μm, high magnification 50μm. (**h**) Histopathological scoring of lung sections (see **Methods**). (**i**) Expression of *Il6* mRNA in lung tissue was determined by real-time PCR. Graph shows *Il6* fold induction compared to uninfected WT mice. (**j**) Levels of IL-6 protein were detected by ELISA. (**k**) Bacterial burden was determined as CFU in tissue homogenates of the right lung lobes. Scatter blots represent individual mice from (**a, e-k**) one or (**b-d**) two pooled experiments. (**f, k**) show one out of two similar experiments. Statistical significance was calculated by

unpaired t-test. Significant p-values were indicated as follows: * $p \leq 0.05$, ** $p \leq 0.01$, *** $p \leq 0.001$, **** $p \leq 0.0001$.